

# Numerical Assessment of Geometric and Load Parameters Associated with Intracranial Aneurysm Formation

Róbert Nagy, Imre Bojtár

Received 31-10-2014, accepted 11-11-2014

## Abstract

Local biomechanical effects play an important role in aneurysm formation and rupture. It is hypothesised that the main governing factors of the pathogenetic process are the temporal variation and spatial distribution of the flow induced wall shear stress (WSS). The present paper investigates the geometry of the carotid bifurcation, a typical location of cerebral aneurysms. Based on patient specific three-dimensional rotation angiography (3DRA) data a parameter study was carried out on a two-dimensional simplified model using the ANSYS commercial framework, describing the blood flow dynamics and the mechanical effects resulting from a physiologically realistic flow. While the geometry-induced surplus of the normal pressure proved to be negligible regarding even the normal diastolic pressure, the WSS and its variation showed significant deviations near the bifurcation apex. Well defined distinct geometrical properties (the lumen area ratio and the bifurcation angle) can be established describing the major impact on the pressure and the WSS enabling us to estimate the potential hazards of a healthy bifurcation.

## Keywords

wall shear stress · bifurcation angle · diameter ratio

## Róbert Nagy

Department of Structural Mechanics, Faculty of Civil Engineering, Budapest University of Technology and Economics, Műegyetem rkp. 3, H-1111 Budapest, Hungary  
e-mail: robert.nagy@mail.bme.hu

## Imre Bojtár

Department of Structural Mechanics, Faculty of Civil Engineering, Budapest University of Technology and Economics, Műegyetem rkp. 3, H-1111 Budapest, Hungary  
e-mail: ibojtar@mail.bme.hu

## 1 Introduction

Aneurysms are localized chronic degenerative disorders of the blood vessels – almost exclusively of arteries – leading to their dilation. The expression itself derives from the ancient Greek term “ἀνεύρυσμα” (aneurysma), meaning widening. These lesions occur predominantly at two – from etiological point of view – different locations, notably in the cranium and in the abdomen. However in our research both variations are considered, the present paper focuses only on the former one. One of the most common and most hazardous locations of these cerebral aneurysms is the carotid bifurcation, a typical branching point of one of the main arteries supplying the brain, where, at the apex, a balloon like (saccular) outpouching is possible to form under certain still obscure conditions. The features of this particular bifurcation serve as the basis for our investigations.

## 2 Motivation

Since most cerebral aneurysms are asymptomatic, only rough approximations can be made to assess their prevalence ratio, which, according to [1], mounts up to 1 - 6% of the population.

The mortality and morbidity ratios of the rupture induced subarachnoid haemorrhage are also remarkably high. 10% of the patients die even before reaching medical attention, another 50% do not survive the first month after the surgery, and around half of the remaining 40% suffer permanent neurological deficits. The treatment of unruptured aneurysms is possible, but it is also a high risk procedure. The two basic methods are the craniotomy and the endovascular coiling having mortality and morbidity ratios of 4 - 10.9% and 1 - 3% [2, 3] against 3.7 - 5.3% and 1.1 - 1.5% [4, 5], respectively.

Taking into consideration the previous data and the fact that incidence ratio of rupture is only 0.5% among those harbouring a cerebral aneurysm, it is essential to provide the most reliable decision strategy possible to neurosurgeons, which, at present, is based on the statistical results of a thorough study [1] involving 4323 patients restricting the decision parameters to a few easily measurable ones, like the age and the diameter of the sac.

At the same time, with the rapid development of in vivo imaging and numerical simulations, a different approach forms the

main area of mechanical related researches in this field, with which, in the near future, the risk of rupture can be estimated more accurately using the framework of patient-specific modelling [6].

In parallel, pioneer investigations [7] are carried out concerning the circumstances of initiation and the biomechanical factors governing the pathogenetic process of these peccant deformations, however, in spite of the elaborate mechanical model of the arterial wall [8] at our disposal, several vital questions necessary to better understand the disease remain unanswered. These are at the forefront of our investigations.

### 3 Problem statement

The evolution of aneurysms is driven by effects resulting from the blood flow. These incorporate both direct mechanical forces and biomechanical stimuli leading to the degradation and remodeling of the arterial wall. The mechanism of this flow related biological process is associated with the shear stress distribution acting on the wall, whereas the exact process still needs to be elucidated in order to explain the remodeling of the tissue, thus enabling a better assessment of the material characteristics of the developed aneurysm wall.

### 4 Purpose

We hypothesise [9], that well defined distinct local geometrical properties (the lumen area ratio and the bifurcation angle) of the bifurcation have a significant impact on the flow induced loads. Our main goal, therefore, is to create a database of the load and stress distribution of the wall as a function of the geometry and hydrodynamic factors. The variable-field shown in Table 1 covers all typical variations; therefore, it could provide a useful and solid basis for comparison and further investigations.

Tab. 1. The parameter field

Parameter field	Range		Step		
	Min	Max	$\Delta$	$n$	$\Sigma n$
Bifurcation angle [°]	15	90	15	6 <sup>2</sup>	6012
Diam. ratio [-]	0.55	0.9	0.05	8 <sup>2</sup>	
Pres. [Pa]	Systole	120	180	20	
	Diastole	80	100	10	3

### 5 Subject of the investigations

This paper analyses the healthy geometrical variation of one of the most common and most hazardous locations of cerebral aneurysms, notably the carotid bifurcation, a typical branching point of one of the main arteries supplying the brain. The junction is at the circle of Willis, where the parent vessel, the internal carotid artery (ICA) divides into two branches, to the middle cerebral artery (MCA) and to the anterior cerebral artery (ACA). A representative geometry obtained by three-dimensional rotation angiography (3DRA) is shown in Fig. 1.

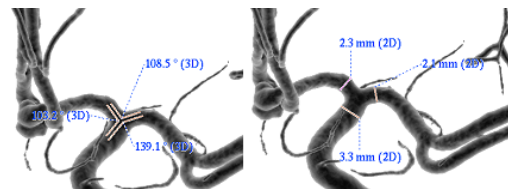


Fig. 1. 3DRA pictures of a healthy carotid bifurcation

#### 5.1 Measurements

We collected the data in Table 2 based on 3DRA measurements of 10 healthy carotid bifurcations carried out on patients of the Hungarian National Institute of Neurosciences. The estimated precision of the readings are 0.1 mm and 5° regarding the length and the angle respectively.

#### 5.2 Model parameters

The length of the main branch ( $L = 20$  mm) and the sub branches ( $l_1 = 20$  mm,  $l_2 = 20$  mm) are fixed along with the main branch diameter ( $D = 4$  mm). The parameter study involves the varying sub branch diameters ( $d_1, d_2$ ) ranging from 50% of the main branch to 90% by 5% increments, and the bifurcation angles ( $\alpha_1, \alpha_2$ ) measured from the axis of the main branch ranging from 15° to 90° by 15°. At the intersection of the edges, in order to evade singularities, a fillet with 1 mm radius is used. The pressure field has the following values: normal 80/120 Hgmm (10.7/16.0 kPa), high 90/140 Hgmm (12.0/18.7 kPa) and critical 100/180 Hgmm (13.3/24.1 kPa).

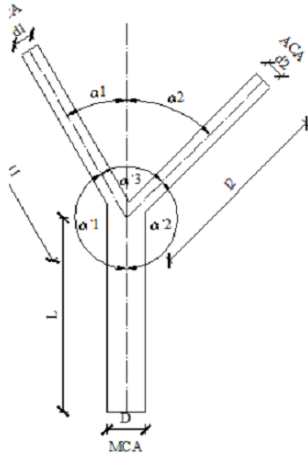
#### 5.3 Approach

For a more precise understanding of the phenomenon, our approach differs from the usual methods, notably, instead of using complex and unique patient specific data, we systematically develop a simplified model of the healthy configuration in an inductive manner. This includes a solid mechanical model of the arterial wall and a hydrodynamic model of the fluid domain starting from the simplest two-dimensional steady state simulation with basic boundary conditions and rigid walls heading towards the more elaborate unsteady simulation with more accurate boundary conditions taking into consideration the material properties of the wall as well. Using these models, we perform a parameter study.

#### 5.4 Modeling stages

The first step is the qualitative investigation of the pressure and WSS solving solely the transport equations of the fluid on a fixed geometry gaining a basic understanding on the load distribution. The second step concerns the global parameters of the bifurcation resulting in its evaluation as a part of the circulatory system. The third milestone turns towards the local features and the spatial distribution of the flow induced loads surrounding the apex. Finally, the time dependency and the influence of the wall elasticity is taken into consideration enabling us to scrutinize both the spatial gradients and time variations of the chosen parameters, which now include the wall stresses, strains

**Tab. 2.** Measured geometric data of 10 healthy carotid bifurcations



	D	d <sub>1</sub>	d <sub>2</sub>	d <sub>1</sub> /D	d <sub>2</sub> /D	d <sub>i</sub> /d <sub>j</sub>	α' <sub>1</sub>	α' <sub>2</sub>	α' <sub>3</sub>	Σα	α <sub>1</sub>	α <sub>2</sub>	age
	[mm]	[mm]	[mm]	[-]	[-]	[-]	[°]	[°]	[°]	[°]	[°]	[°]	[year]
1	3.3	2.4	2.0	0.727	0.606	1.200	93	134	129	356	87	46	62
2	2.8	2.0	1.6	0.714	0.571	1.250	148	102	109	359	33	78	49
3	3.3	2.5	2.4	0.758	0.727	1.042	114	75	115	305	66	105	56
4	2.1	1.6	1.5	0.762	0.714	1.067	150	114	100	365	30	66	47
5	4.3	2.9	2.4	0.674	0.558	1.208	142	85	111	337	38	95	39
6	3.0	2.0	2.0	0.667	0.667	1.000	135	93	113	341	45	87	67
7	2.5	2.2	1.5	0.880	0.600	1.467	154	77	129	361	26	103	55
8	3.5	2.3	2.4	0.657	0.686	1.043	128	87	112	327	52	93	65
9	3.3	2.3	2.1	0.697	0.636	1.095	139	103	109	351	41	77	70
10	2.9	2.4	2.4	0.828	0.828	1.000	131	96	132	359	49	84	45
min.	2.1	1.6	1.5	0.657	0.558	1.000	93	75	100	305	26	46	39
max.	4.3	2.9	2.4	0.880	0.828	1.467	154	134	132	365	87	105	70
avg.	3.1	2.3	2.0	0.736	0.659	1.137	133	97	116	346	47	83	55.5

and displacements, together with the effect of the interaction of the solid and the fluid part.

### 5.5 Model description

For the above described geometries, the most complex model presented in this paper is a two-dimensional unsteady, fully coupled fluid structure interaction (FSI) simulation, where the fluid and the solid domains are handled separately with the most suitable numerical procedure, the finite volume and the finite element method, respectively, both available in the ANSYS 14.0 numerical simulation software package. The FSI is handled in the ANSYS Workbench framework, where the solution sequence is governed by the finite volume method.

### 5.6 General assumptions

Averaging the sums of the angles between the three branches ( $\alpha_m = 346^\circ \pm 19^\circ$ ), the assumption of a much simpler planar geometry seems to be acceptable, by which the secondary flow formations are neglected, therefore, in the future, it is necessary to be compared with the 3D models. The curvature of the branches are also neglected, noting that as a best practice in 3D models, the first preceding bend should also be incorporated in the simulation. The geometry induced mechanical loads being at the focal point of this paper, the implementation of the biologic processes is not considered and the layered structure of the wall, the anisotropy due to the collagen fibres, and the local variations of material properties due to the wall degradation are neglected as well.

### 5.7 Fluid domain

Although blood is a dispersed fluid, and as such, non-Newtonian behaviour (yield stress and shear thinning) can be observed at locations of low shear rate, studies [10] have shown that in cases similar to ours (in arteries of diameter larger than 0.5 mm) it has no significant effect, therefore the widely accepted incompressible Newtonian fluid model is adopted. The

flow, in accordance with the experiences, is laminar. The temperature is constant; therefore the energy transport equation can be omitted. The gravitational forces and the inertia forces due to the changes in the state of motion of the head are neglected. The most important dimensionless quantities of the flow are the peak Reynolds number with respect to the vessel diameter ( $Re = 938$ ), the Dean number ( $De = 1083$ ), and the Womersley number ( $Wo = 6.63$ ) show that the flow is laminar, the secondary flow formations from the vessel curvature are stable, and the pulsatile velocity profile varies significantly with time.

With the above assumptions, the following governing transport equations hold for the mass (1) and the momentum (2):

$$\frac{\partial u_i}{\partial x_i} = 0, \quad (1)$$

$$\rho^f \cdot \left[ \frac{\partial u_i}{\partial t} + (u_j - u_j^g) \frac{\partial u_i}{\partial x_j} \right] = -\frac{\partial p}{\partial x_i} + \mu^f \frac{\partial^2 u_i}{\partial x_j \partial x_j}, \quad (2)$$

where  $\rho^f = 1050 \text{ kg/m}^3$  is the blood density,  $\mu^f = 0.003 \text{ Pas}$  is the dynamic viscosity respectively. In the arbitrary Lagrangian – Eulerian (ALE) formulation,  $(u_j - u_j^g)$  is the relative velocity of the fluid with respect to the moving coordinate velocity.

At the inlet boundary the spatial distribution of the velocity profile is assumed to be parabolic prescribed far enough from the bifurcation to enable the realistic profile to develop without distorting the data at the apex. For the three consecutive pulsatile flow cycles considered, the time dependency is imposed by the first 4 harmonics of the Fourier spectrum of unified data acquired by Doppler ultrasound measurements, the cardiac cycle duration being 0.8 s and the peak flow velocity 1 m/s. For further details of the waveform characteristics see: [11].

At the outlet boundary, modelling the resistance of the following blood vessels, a porous zone is applied having two parameters (the constant momentum source and outlet pressure) with the calibration of which the maximal (systolic) and the minimal (diastolic) pressure inside the fluid domain can be adjusted. At the wall no-slip condition is applied. The code being unable

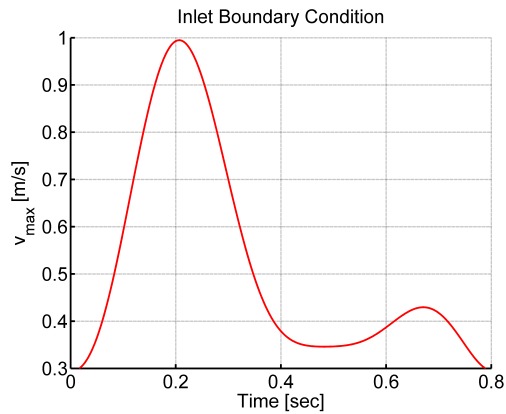


Fig. 2. Velocity profile at the inlet

to deal with two-dimensional grids, the geometry is extruded perpendicularly to its plane by 0.1 mm forming a single layer of elements. To acquire the planar flow properties a symmetry boundary condition is used on both sides.

The governing equations are solved with the ANSYS CFX 14.0 software, which utilizes the finite volume method. On an unstructured grid, the discretised transport equations are solved with a high resolution advection scheme, and the pressure-velocity coupling is formulated by the co-located 4<sup>th</sup> order Rhie–Chow algorithm. The implicit second order backward Euler scheme is used for the temporal formulation with a constant time step of 0.01 s within each of which a maximum iteration number of 300 is prescribed producing residuals smaller than  $10^{-7}$ . The verification mesh independence on 6 grid sizes revealed that the maximum face size of 0.2 mm in general with inflation layers of 1.5 geometrical growth ratio at the wall produces relative error in both pressure and WSS less than 5%.

### 5.8 Solid domain

The arterial wall is considered to be homogeneous, isotropic, obeying the linear-elastic Hooke's law:

$$\sigma_{ij} = D_{ijkl} \cdot \varepsilon_{kl} , \quad (3)$$

$$D_{ijkl} = E \cdot \left[ \frac{\nu}{(1 + \nu) \cdot (1 - 2\nu)} \cdot \delta_{ij}\delta_{kl} + \frac{1}{2(1 - 2\nu)} (\delta_{ki}\delta_{lj} + \delta_{kj}\delta_{li}) \right] , \quad (4)$$

with the compatibility equation:

$$\varepsilon_{ij} = \frac{1}{2} \left( \frac{\partial d_i}{\partial x_j} + \frac{\partial d_j}{\partial x_i} \right) , \quad (5)$$

where  $\sigma_{ij}$  and  $\varepsilon_{ij}$  are the solid stress and strain tensors respectively,  $d_i$  is the displacement  $E = 3.6$  MPa is the elastic modulus,  $\nu = 0.49$  is the Poisson's ratio. The wall thickness is  $w = 0.2$  mm, the density of the arterial wall is  $\rho^s = 1050$  kg/m<sup>3</sup>.

For the solid domain a Lagrangian coordinate system is adopted, so the governing momentum conservation equation can

be formulated as:

$$\rho^s \cdot \frac{\partial^2 d_j^s}{\partial t^2} - \frac{\partial \sigma_{ij}}{\partial x_j} = 0 . \quad (6)$$

Exploiting the linear relation between the forces acting on a thin cylindrical shell and its normal displacements, the curvature in the direction perpendicular to the plane of the analysis can be taken into account with the adaptation of an elastic Winkler type foundation:

$$k = \frac{w \cdot E}{r^2} , \quad (7)$$

$r$  being the radius of the lumen. The pressure of the cerebrospinal fluid and the surrounding tissues ( $p_w = 400$  Pa) is constant according to the Monroe–Kelly hypothesis. All the solid parts are fixed in the direction perpendicular to the plane of the analysis. At the inlet and at the outlets only displacements in the plane of the cross section are allowed.

The governing equations are solved with an implicit finite element method using the ANSYS Mechanical code. Since the geometry is three dimensional, the 8-node quadratic SHELL 281 element with side length of 0.5 mm is chosen for the geometrical discretisation of the solid part.

## 6 Results

### 6.1 Qualitative investigation

Fig. 3 shows the results of a steady state simulation of a symmetric T-shaped bifurcation with rigid walls, without the momentum source at the outlet.

On the first hand, it can readily be observed, that on the top wall the pressure is maximal at the stagnation point – as one would expect – with the value ( $p_{max} = 480$  Pa) approximately equal to dynamic pressure at the center point of the inlet boundary according to the corresponding stream line. Note the rapid decrease to normal in a few centimetres. Albeit, this geometry induced surplus is of two orders smaller in magnitude than the normal diastolic pressure ( $10^4$  Pa), and appears to be negligible compared to the hypertonic overpressure, which can rise up to even higher than the previous value, it has to be kept in mind that the long term repetitive effects are possible to cause wall degradation and residual deformations. On the other hand, the WSS shows significant spatial variations with minimum occurring at the stagnation point, and maxima surrounding it at a distance (9.6 mm) of the recorded aneurysm neck widths. It is not clear whether the high or low WSS, representing high and low flow conditions, or its rapid variation is to blame for the NO mediated biological effects driving the pathogenesis, but the truth is believed to lie somewhere in-between. Mostly the high WSS ( $> 40$  Pa) [12] is regarded as a major factor in aneurysm growth [13], while the rupture is associated with low WSS ( $< 2$  Pa) [14]. Due to the bifurcation the WSS shows significant spatial variation around the expected location of aneurysm formation, with maximal values (23.76 Pa) being an order of magnitude higher

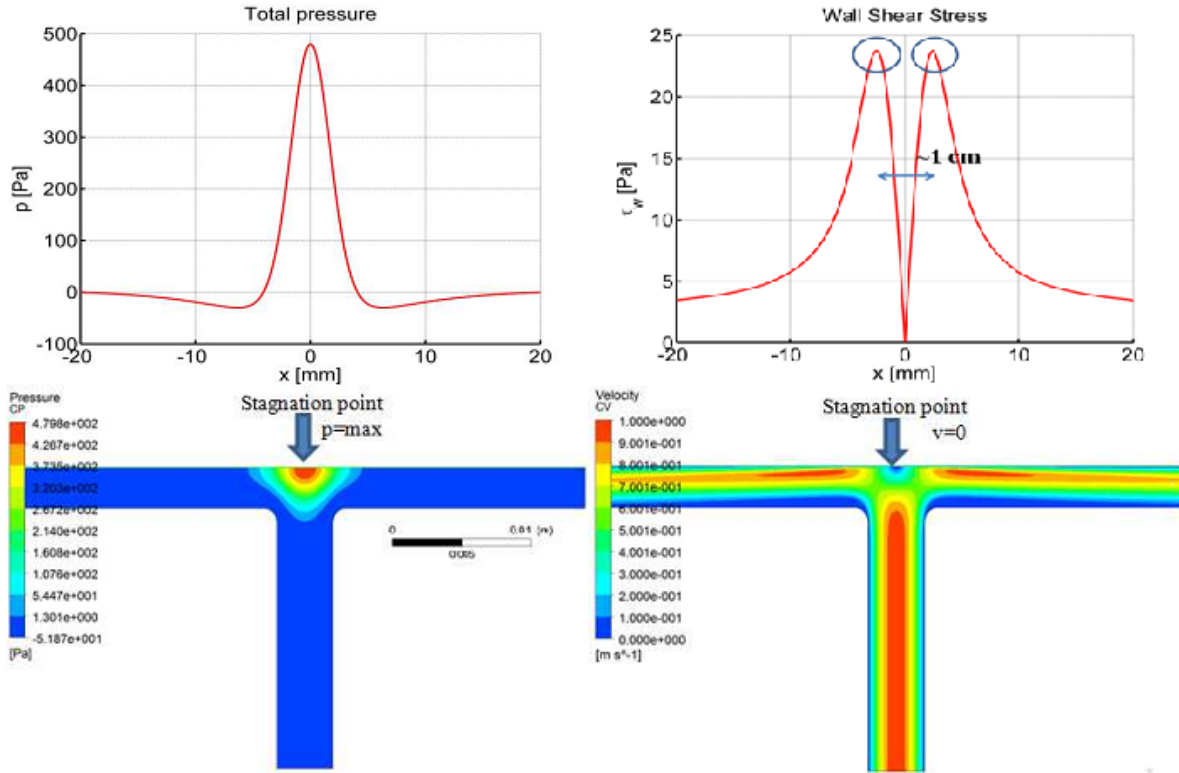


Fig. 3. Pressure drop against the inlet/outlet diameter ratio and the bifurcation angle

than those of the normal sections (2.85 Pa), and minimal values approaching zero. Note that the pressure profile at the inlet and the radius of the fillet at the bifurcation peak could also have an effect on the load distribution, which need to be examined in the future.

## 6.2 Global parameters

Sweeping through the geometrically symmetric part of the described parameter field using the previous model, it is possible to determine the optimal shape where the pressure drop characterizing the resistance of the system is the smallest. This is depicted in Fig. 4.

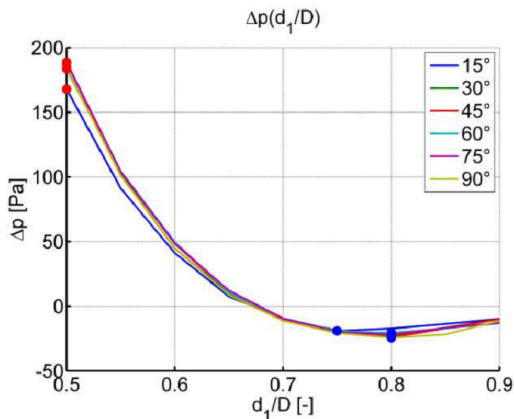


Fig. 4. Pressure drop against the inlet/outlet diameter ratio and the bifurcation angle

The pressure drop varies slightly (with magnitude of maximum 5% occurring near  $\alpha = 60^\circ$ ) with the bifurcation angle, whereas the diameter ratio proves to be of high importance

defining an optimal geometry with minimal resistance between the values 0.75 and 0.80, which, comparing to the data in Table 2, and assuming that nature seeks for the optimum, can be regarded as a physiological validation of the model. For diameter ratios higher than 0.68 the inlet pressure becomes larger than that at the outlet, i.e. the system acts like a diffuser, leading to high energy losses. Introducing the dissipation ratio in (8) and (9), which measures the ratio of the energy dissipated by the system and the energy supplied to it, similar results yield from our investigations.

$$\eta_{dis} = \frac{\sum \dot{E}_{in} - \sum \dot{E}_{out}}{\sum \dot{E}_{in}}, \quad (8)$$

$$\dot{E} = \dot{W}_p + \dot{E}_{kin} = \sum_k \int_{A_k} \left( p + \frac{\rho \cdot u_i^2}{2} \right) \cdot u_i \cdot n_i dA_k. \quad (9)$$

Here  $n_i$  denotes the components of the surface unit normal. It is worth noting that the three-dimensional model might provide different results, because there the cross sectional area is a quadratic function of the diameter.

## 6.3 Local Features

A good approximation of the peak static pressure is the sum of the pressure drop and the dynamic pressure at the midpoint of the inlet boundary, thus having the same tendencies as the pressure drop component, still remaining small compared to the normal diastolic pressure. In contrast to the pressure, the peak WSS shows only slight dependency on the diameter ratio (the

decrease in the diameter ratio from 0.9 to 0.5 induces only 5-10% growth), but becomes sensitive to the bifurcation angle as seen in Fig. 5. The sharper the angle, the higher the  $WSS_{max}$  is. The graph comprises of two linear parts. When  $\alpha > 60^\circ$  holds, the  $WSS_{max}$  is almost constant, while, with  $\alpha$  decreasing from  $60^\circ$  it rises steeply to 60.5 Pa, a value 2.36 times bigger than that of the T-shaped geometry. Note that it also exceeds the limit of wall degradation given by [12]. Looking at the graph in Fig. 6, it can be derived that the peak WSS remains below approximately 40 Pa if the geometric sum of the two bifurcation angles exceeds  $90^\circ$ .

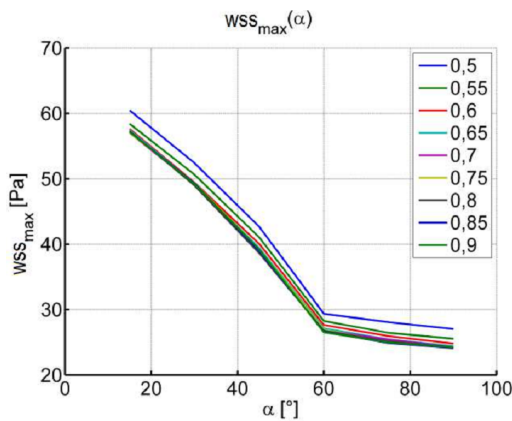


Fig. 5.  $WSS_{max}$  against the inlet/outlet diameter ratio

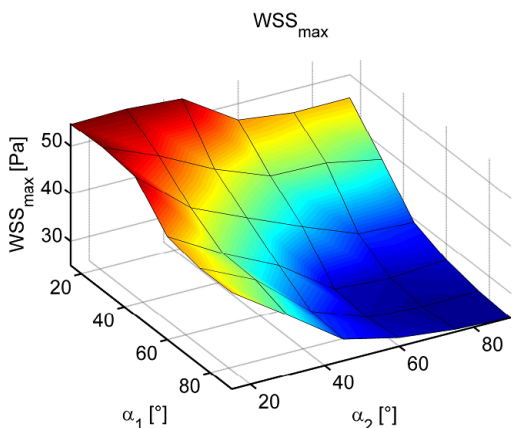


Fig. 6.  $WSS_{max}$  against the bifurcation angle.

#### 6.4 Time dependency

In the unsteady case, the porous zone applied at the outlet provides a physiologically realistic pressure field. In good accordance with the former conclusions the pressure imposed at the top wall (Fig. 7) exhibits large temporal variations, but with small spatial gradients due to the similarly small geometric surplus (3.7%). The WSS (Fig. 8) has its peak near the aneurysm neck in space occurring at the time of the systole.

#### 7 Fluid structure interaction

The application of the FSI procedure allows us now to examine the wall stresses, strains and displacements, together with the effect of the compliant wall on the loads exerted on it by the

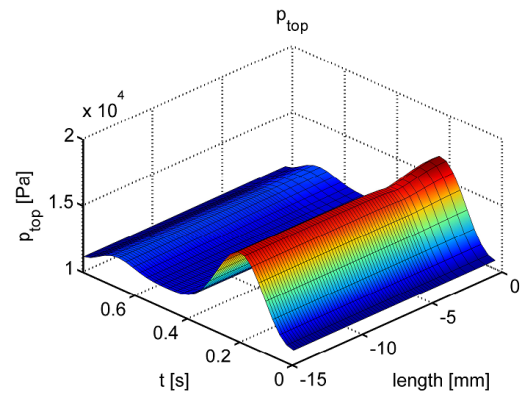


Fig. 7. Pressure distribution on the top wall during a cardiac cycle

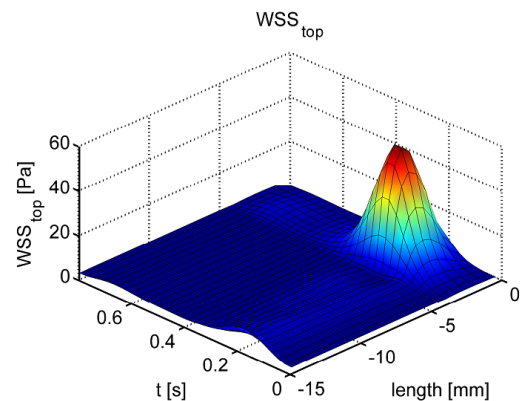


Fig. 8. WSS distribution on the top wall during a cardiac cycle

blood flow. Typical characteristics are presented in the following. Concerning the loads, the elasticity of the wall decreases the  $WSS_{max}$  approximately by 10-15%, and increases the peak pressure by 3-5%. The wall displacements showed good agreement with the realistic measurements being around 5% of the diameter ratio. This also can be considered as the validation of the model, especially of the Winkler type foundation model. The example showing the magnitudes of the stress tensor at the stagnation point is written in (10).

$$\sigma = \begin{bmatrix} 1.2 & 0.022 & 0 \\ 0.022 & 18.4 & 0 \\ 0 & 0 & 266.3 \end{bmatrix} kPa, \quad (10)$$

Since even the highest stress component is an order of magnitude smaller than the one-dimensional limit stress of the healthy arterial wall (cca.  $\sigma_{lim} = 3 \text{ MPa}$ ), it is to be concluded that solely the direct, local, short term mechanical effects do not account for the aneurysm formation, and, however the long term pulsatile loading can deteriorate the wall, it is necessary to include biological effects into our studies.

#### 8 Conclusions

Mechanical stimuli play a vital role in the process of aneurysm initiation, growth, and rupture. This paper investigated the impact of certain important geometrical parameters (the bifurcation angle and the outlet/inlet diameter ratio) on the flow induced load parameters (namely the pressure and the WSS)

imposed on the arterial wall in case of a healthy carotid bifurcation model, a representative location of intracranial aneurysm formation. It is observed that the geometry-induced surplus of the normal pressure is negligible regarding even the normal diastolic pressure, while the WSS and its variation showed significant deviations near the bifurcation apex. The first having a peak at the stagnation point vanishes rapidly with distance, the second exhibits two maxima approximately at the locations of the aneurysm neck, surrounding its minima at the ram point. The parameter study revealed that the pressure field and the WSS depend mainly on the diameter ratio and the bifurcation geometry, respectively. The optimal geometry is achieved at diameter ratio between 0.75 and 0.80, and at opening angles larger than 90°. The unsteady models showed that the spatial gradients of the pressure are small, while the temporal fluctuation is significant, whereas in case of the WSS both gradients are high. The FSI method made it possible to scrutinize the effect of the solid wall, in this way the maximal pressure at the stagnation point typically increased by 3–5%, the peak WSS decreased by 10–15%. The wall displacement agrees well with the experimental values. These mechanical loads leaving the stress field an order of magnitude smaller than the limit stress of the arterial wall cannot be accounted for its degradation in a short term, but considering the long term pulsatile effect it may lead to aneurysm formation, however it is inevitable to incorporate a more elaborate material model in our simulations capable of following the biomechanical degradation and remodelling of the arterial wall.

## 9 Future prospects

Noting that the results of this model are in good agreement with the experimental values, the limitations of the two-dimensional geometry have to be borne in mind. One of the main extensions of the investigations presented is the development of a similar three-dimensional model, which is now at the final stage.

In parallel, using this as a foundation, and cooperating with surgeons, physiologists and histologists, we aim to develop a material model on a microstructural foundation that is capable of describing the mechanical, biological and chemical behaviour and degradation of the tissue. Additionally, by integrating this into numerical models, we will be able to follow the evolution and rupture of the aneurysms in the future gaining a better understanding of the phenomenon.

## References

- 1 **Wiebers DO**, *Unruptured intracranial aneurysms: natural history, clinical outcome, and risks of surgical and endovascular treatment*, *The Lancet*, **362**(9378), (2003), 103–110, DOI 10.1016/S0140-6736(03)13860-3.
- 2 **Claiborne Johnston S, Wilson CB, Halbach VV, Higashida RT, Dowd CF, McDermott MW, Applebury CB, Farley TL, Gress DR**, *Endovascular and surgical treatment of unruptured cerebral aneurysms: Comparison of risks*, *Annals of Neurology*, **48**(1), (2000), 11–19, DOI 10.1002/1531-8249(200007)48:1<11::AID-ANA4>3.3.CO;2-M.

- 3 **Campi A, Ramzi N, Molyneux AJ, Summers PE, Kerr RSC, Sneade M, Yarnold JA, Rischmiller J, Byrne JV**, *Retreatment of Ruptured Cerebral Aneurysms in Patients Randomized by Coiling or Clipping in the International Subarachnoid Aneurysm Trial (ISAT)*, *Stroke*, **38**(5), (2007), 1538–1544, DOI 10.1161/STROKEAHA.106.466987.
- 4 **Johnston SC, Zhao S, Dudley RA, Berman MF, Gress DR, Kassell NF, Lanzino G**, *Treatment of Unruptured Cerebral Aneurysms in California Editorial Comment : Unruptured Intracranial Aneurysms: In Search of the Best Management Strategy*, *Stroke*, **32**(3), (2001), 597–605, DOI 10.1161/01.STR.32.3.597.
- 5 **Juvela S, Bederson J**, *Recommendations for the Management of Patients With Unruptured Intracranial Aneurysms Response*, *Stroke*, **32**(3), (2001), 815–816, DOI 10.1161/01.STR.32.3.815.
- 6 **Cebral JR, Castro MA, Burgess JE, Pergolizzi RS, Sheridan MJ, Putman CM**, *Characterization of cerebral aneurysms for assessing risk of rupture by using patient-specific computational hemodynamics models*, *American Journal of Neuroradiology*, **26**(10), (2005), 2550–2559.
- 7 **Watton PN, Selimovic A, Raberger NB, Huang P, Holzapfel GA, Ventičkos Y**, *Modelling evolution and the evolving mechanical environment of saccular cerebral aneurysms*, *Biomechanics and Modeling in Mechanobiology*, **10**(1), (2011), 109–132, DOI 10.1007/s10237-010-0221-y.
- 8 **Holzapfel GA, Gasser TC, Ogden RW**, *A new constitutive framework for arterial wall mechanics and a comparative study of material models*, *Journal of elasticity and the physical science of solids*, **61**(1-3), (2000), 1–48.
- 9 **Nagy R**, *Numerical evaluation of mechanical parameters inducing the formulation of intracranial aneurysms*, 2011. MSc thesis in Hungarian (Agyi aneurizmák kialakulásáért felelős mechanikai paraméterek értékelése numerikus módszerekkel).
- 10 **Perktold K, Peter R, Resch M**, *Pulsatile non-Newtonian blood flow simulation through a bifurcation with an aneurysm*, *Biorheology*, **26**(6), (1988), 1011–1030.
- 11 **Holdsworth DW, Norley CJD, Frayne R, Steinman DA, Rutt BK**, *Characterization of common carotid artery blood-flow waveforms in normal human subjects*, *Physiological Measurement*, **20**(3), (1999), 219, DOI 10.1088/0967-3334/20/3/301.
- 12 **Fry DL**, *Acute Vascular Endothelial Changes Associated with Increased Blood Velocity Gradients*, *Circulation Research*, **22**(2), (1968), 165–197, DOI 10.1161/01.RES.22.2.165.
- 13 **Tateshima S, Murayama Y, Villablanca JP, Morino T, Nomura K, Tanishita K, Vinuela F**, *In Vitro Measurement of Fluid-Induced Wall Shear Stress in Unruptured Cerebral Aneurysms Harboring Blebs*, *Stroke*, **34**(1), (2003), 187–192, DOI 10.1161/01.STR.0000046456.26587.8B.
- 14 **Shojima M, Oshima M, Takagi K, Torii R, Hayakawa M, Katada K, Morita A, Kirino T**, *Magnitude and Role of Wall Shear Stress on Cerebral Aneurysm: Computational Fluid Dynamic Study of 20 Middle Cerebral Artery Aneurysms*, *Stroke*, **35**(11), (2004), 2500–2505, DOI 10.1161/01.STR.0000144648.89172.0f.